Comput Geosci (2007) 11:207–218
DOI 10.1007/s10596-007-9043-0

ORIGINAL PAPER

A computational method for approximating a Darcy–Stokes system governing a vuggy porous medium

Todd Arbogast · Dana S. Brunson

Received: 16 June 2005 / Accepted: 9 January 2007 / Published online: 21 February 2007

Abstract We develop and analyze a mixed finite element method for the solution of an elliptic system modeling a porous medium with large cavities, called vugs. It consists of a second-order elliptic (i.e., Darcy) equation on part of the domain coupled to a Stokes equation on the rest of the domain, and a slip boundary condition (due to Beavers–Joseph–Saffman) on the interface between them. The tangential velocity is not continuous on the interface. We consider a 2-D vuggy porous medium with many small cavities throughout its extent, so the interface is not isolated. We use a certain conforming Stokes element on rectangles, slightly modified near the interface to account for the tangential discontinuity. This gives a mixed finite element method for the entire Darcy–Stokes system with a regular sparsity pattern that is easy to implement, independent of the vug geometry, as long as it aligns with the grid. We prove optimal global first-order L^2 convergence of the velocity and pressure, as well as the velocity gradient in the Stokes domain. Numerical results verify these rates of convergence and even suggest somewhat better convergence in certain situations. Finally, we present a lower dimensional space that uses Raviart–Thomas elements in the Darcy domain and uses our new modified elements near the interface in transition to the Stokes elements.

Keywords Beavers–Joseph boundary condition · Darcy–Stokes system · error estimates · mixed finite elements · vuggy porous media

T. Arbogast (✉) · D. S. Brunson
Department of Mathematics,
The University of Texas at Austin, 1 University Station
C1200, Austin, TX 78712, USA
e-mail: arbogast@ices.utexas.edu

D. S. Brunson
e-mail: dbrunson@math.utexas.edu

T. Arbogast · D. S. Brunson
Institute for Computational Engineering and Sciences,
The University of Texas at Austin, 1 University Station
C0200, Austin, TX 78712, USA

1 Introduction

We consider the approximation of the equations governing the flow of an incompressible fluid in a medium $\Omega \subset \mathbb{R}^2$ composed of a porous material that also contains relatively large cavities. Such cavities are called *vugs* in the geological literature. They occur ubiquitously throughout, for example, most carbonate rock formations. Although small, vugs can significantly increase both the effective porosity and permeability of the medium.

Since only low Reynold's number flow is to be expected, the system is governed in the rock matrix $\Omega_d \subset \Omega$ by a second-order elliptic equation representing Darcy's law and mass conservation, and in the vugs $\Omega_s = \Omega \setminus \bar{\Omega}_d$ by the Stokes equation, with the Beavers–Joseph–Saffman boundary condition [5, 21] on the interface between the two regions $\Gamma = \partial\Omega_d \cap \Omega_s$. The system is difficult to approximate because the Darcy and Stokes solutions have very different regularity properties, and, more importantly, the tangential velocity may be discontinuous on the Darcy–Stokes interface Γ.

Previous studies have developed numerical techniques appropriate to the case where the porous medium and the open (vuggy) region are well sepa-

rated [14, 19, 22]. However, these techniques are not so readily adapted to the case of a vuggy medium, for which there is no distinct separation between the vuggy regions and the porous rock, i.e., to the case where the vugs and porous matrix are essentially intertwined everywhere. For example, Layton et al. [19] used a Lagrange multiplier on the interface Γ to both aid in the approximation of the Beavers–Joseph–Saffman boundary condition and to allow the use of existing Darcy and Stokes flow simulators in a domain–decomposition (Ω_d and Ω_s) iterative technique. They also provided a very thorough error analysis of their underlying method and the equations in general. However, this approach is not so useful when Γ is large because the size of the Lagrange multiplier space would preclude efficient solution.

The approach taken here is to design a finite element that is appropriate for both the Stokes and Darcy regions of the domain. The rationale is that then an efficient code can be written with little regard to the nature of the underlying equations, i.e., whether an element lies in Ω_s or Ω_d. For simplicity, we use conforming elements. Since the Stokes equations are necessarily a saddle point system, we consider the second-order elliptic Darcy equations in mixed form. Stokes approximation requires that the fluid velocities be approximated in $(H^1(\Omega))^2$, which is more restrictive than the Darcy simulation requires. Mixed methods approximate velocities only in the space $H(\mathrm{div}) = \{\mathbf{u} \in (L^2)^2 : \nabla \cdot \mathbf{u} \in L^2\}$ [11, 20]. This requires only the (weak) continuity of normal velocity components, whereas Stokes requires both normal and tangential components to be (weakly) continuous. We thereby restrict ourselves to using a finite element appropriate for Stokes simulation that simultaneously works well for Darcy simulation. We adopt the low-order space due to Fortin [13]. This space and higher order generalizations have been shown by Arbogast and Wheeler [3] to approximate well second-order elliptic systems. To approximate the combined Darcy–Stokes system, since the tangential velocity may be discontinuous, this finite element space must be modified near Γ, but the modification is relatively minor and easily handled in a computer code. In principle, our results should extend to 3-D elements. Since this has not been tested, we present only the 2-D case here.

The outline of the rest of the paper follows. In the next section, we state in detail the governing equations and a mixed variational form suitable for finite element approximation. In Section 3, we define our finite element spaces as a small modification of the Fortin spaces, and then the finite element method follows immediately. In Section 4, we present a π projection operator for the velocity and examine its properties. This operator is used in Section 5, where we present an a priori error analysis. We show that the method approximates both the true velocity and pressure to the optimal first order in the standard energy norm. That is, the Stokes velocity error is measured in the $(H^1)^2$ norm, the Darcy velocity error is measured in $(L^2)^2$, and the pressure error is measured in L^2. We present the results of several numerical experiments to verify these rates of convergence in Section 6. Since these test cases lead to very ill-conditioned linear systems, in Section 6, we also discuss our solution strategy. Finally, in the last section, we consider a finite element space with lower total dimension by replacing the Fortin elements by Raviart–Thomas [20] elements on Darcy elements away from the Darcy–Stokes interface.

We close the introduction with a remark about simulation of flow in vuggy media. When the medium is large in extent, such as an aquifer or petroleum reservoir, it is not reasonable to solve the Darcy–Stokes system over the entire domain for several reasons. First, there are inadequate data regarding the geometry of the vugs over the many square-kilometer areal extent of the domain. Second, at the centimeter resolution that would be required to resolve the vugs, the problem would be computationally intractable. Finally, the data generated would be much too detailed to be of use in engineering analyses, where only meter-scale average flows would be used.

Recently, Arbogast and Lehr [2] derived from the microscale model of the next section a macroscopic model using the mathematical theory of homogenization [6, 16, 17, 23]. The theoretical prediction is that Darcy flow results at the macroscale. What is important here is that an expression for the effective permeability is also derived. This expression involves the solution of a Darcy–Stokes system on a representative cell involving the vug geometry (except that periodic boundary conditions must be imposed). The numerical method of this paper is suitable for solving this cell problem, and thereby allowing one to obtain effective permeabilities for vuggy media.

2 The governing equations

In all of Ω, denote the fluid velocity by $\mathbf{u}$ and the pressure by p. We will often need to distinguish between these quantities on Ω_s or Ω_d, and especially their traces on Γ. Thus, let

$$\mathbf{u}_s = \mathbf{u}|_{\Omega_s}, \quad \mathbf{u}_d = \mathbf{u}|_{\Omega_d}, \quad p_s = p|_{\Omega_s}, \quad \text{and} \quad p_d = p|_{\Omega_d}.$$

Let $\mu > 0$ be the fluid viscosity, $K \in L^\infty(\Omega)$ the uniformly positive permeability of the porous rock matrix,

$\alpha > 0$ the Beavers–Joseph slip coefficient, $q \in L^2(\Omega)$ an external source or sink term (satisfying the compatibility condition that its average over Ω vanishes), and $f \in (L^2(\Omega))^2$ a term related to body forces such as gravity. Let ν be the outer unit normal to $\partial\Omega$, and on Γ, let it be the outer unit normal to $\partial\Omega_s$. Let τ be a unit tangent to Γ, and let D be the symmetric gradient, i.e., $D(\psi)$ is the matrix $\frac{1}{2}\left(\frac{\partial \psi_i}{\partial x_j} + \frac{\partial \psi_j}{\partial x_i}\right)$. Then the governing equations are [5, 18, 21].

Vuggy region (Stokes equations)

$$-2\mu\nabla \cdot D\mathbf{u} + \nabla p = f \quad \text{in } \Omega_s\,, \tag{2.1}$$

$$\nabla \cdot \mathbf{u} = q \quad \text{in } \Omega_s\,, \tag{2.2}$$

Rock matrix (Darcy equations)

$$\mu K^{-1}\mathbf{u} + \nabla p = f \quad \text{in } \Omega_d\,, \tag{2.3}$$

$$\nabla \cdot \mathbf{u} = q \quad \text{in } \Omega_d\,, \tag{2.4}$$

Interface

$$\mathbf{u}_s \cdot \nu = \mathbf{u}_d \cdot \nu \quad \text{on } \Gamma\,, \tag{2.5}$$

$$2\nu \cdot D\mathbf{u}_s \cdot \tau = -\alpha K^{-1/2}\mathbf{u}_s \cdot \tau \quad \text{on } \Gamma\,, \tag{2.6}$$

$$2\mu\nu \cdot D\mathbf{u}_s \cdot \nu = p_s - p_d \quad \text{on } \Gamma\,, \tag{2.7}$$

Outer boundary

$$\mathbf{u}_s = 0 \quad \text{on } \partial\Omega \cap \partial\Omega_s\,, \tag{2.8}$$

$$\mathbf{u}_d \cdot \nu = 0 \quad \text{on } \partial\Omega \cap \partial\Omega_d\,. \tag{2.9}$$

The interface conditions represent continuity of mass flux Eq. 2.5, the Beavers–Joseph–Saffman condition on the tangential stress Eq. 2.6, and the continuity of normal stress Eq. 2.7. Note that because we do not assume a vanishing divergence in Eq. 2.2, we must pose Eq. 2.1 in terms of the symmetric gradient.

A suitable variational form is posed with the velocity $\mathbf{u}$ in the space

$$\mathbf{V} = \{\mathbf{v} \in H(\mathrm{div};\Omega) : \mathbf{v}_s = \mathbf{v}|_{\Omega_s} \in (H^1(\Omega_s))^2,$$
$$\mathbf{v} \cdot \nu = 0 \text{ on } \partial\Omega, \mathbf{v} = 0 \text{ on } \partial\Omega_s \cap \partial\Omega\}\,,$$

in which the outer boundary condition is imposed and pressure p in the space $W = L^2(\Omega)/\mathbb{R}$. Note that the vector valued functions in $\mathbf{V}$ have (weakly) continuous normal components on Γ [11], but that the tangential components need not agree. Let $(\cdot,\cdot)$ denote the $L^2(\Omega)$, $(L^2(\Omega))^2$, or $(L^2(\Omega))^{2\times 2}$ inner product or duality pairing, as appropriate. Also, $(\cdot,\cdot)_\ell$, $\ell = \mathrm{s}, \mathrm{d}$, will be the same with Ω replaced by Ω_ℓ, and $\langle\cdot,\cdot\rangle$ will be the $L^2(\Gamma)$ inner product or duality pairing.

To derive the variational form, for $\mathbf{v} \in \mathbf{V}$, the left side of Eq. 2.1 is manipulated as

$$-2\mu(\nabla \cdot D\mathbf{u}, \mathbf{v})_s + (\nabla p, \mathbf{v})_s = 2\mu(D\mathbf{u}, D\mathbf{v})_s - 2\mu\langle\nu \cdot D\mathbf{u}_s, \mathbf{v}\rangle - (p, \nabla \cdot \mathbf{v})_s + \langle p_s, \mathbf{v} \cdot \nu\rangle\,,$$

and the first interface term on the right is further manipulated as

$$\begin{aligned}-2\mu\langle\nu \cdot D\mathbf{u}_s, \mathbf{v}\rangle &= -2\mu\langle\nu \cdot D\mathbf{u}_s \cdot \nu, \mathbf{v} \cdot \nu\rangle \\ &\quad - 2\mu\langle\nu \cdot D\mathbf{u}_s \cdot \tau, \mathbf{v}_s \cdot \tau\rangle \\ &= -\langle p_s - p_d, \mathbf{v} \cdot \nu\rangle \\ &\quad + \mu\langle\alpha K^{-1/2}\mathbf{u}_s \cdot \tau, \mathbf{v}_s \cdot \tau\rangle\,,\end{aligned}$$

using the interface conditions (2.6) and (2.7). Thus, Eq. 2.1 becomes

$$2\mu(D\mathbf{u}, D\mathbf{v})_s + \mu\langle\alpha K^{-1/2}\mathbf{u}_s \cdot \tau, \mathbf{v}_s \cdot \tau\rangle - (p, \nabla \cdot \mathbf{v})_s + \langle p_d, \mathbf{v} \cdot \nu\rangle = (f, \mathbf{v})_s\,. \tag{2.10}$$

Similarly, Eq. 2.3 is manipulated as

$$\mu(K^{-1}\mathbf{u}, \mathbf{v})_d + (\nabla p, \mathbf{v})_d = \mu(K^{-1}\mathbf{u}, \mathbf{v})_d - (p, \nabla \cdot \mathbf{v})_d - \langle p_d, \mathbf{v} \cdot \nu\rangle = (f, \mathbf{v})_d\,, \tag{2.11}$$

since ν points into Ω_d. Thus, the entire system (2.1)–(2.9) for $(\mathbf{u}, p) \in \mathbf{V} \times W$ becomes, for test functions $(\mathbf{v}, w) \in \mathbf{V} \times W$,

$$2\mu(D\mathbf{u}, D\mathbf{v})_s + \mu\langle\alpha K^{-1/2}\mathbf{u}_s \cdot \tau, \mathbf{v}_s \cdot \tau\rangle + \mu(K^{-1}\mathbf{u}, \mathbf{v})_d - (p, \nabla \cdot \mathbf{v}) = (f, \mathbf{v})\,, \tag{2.12}$$

$$(\nabla \cdot \mathbf{u}, w) = (q, w)\,. \tag{2.13}$$

Note that Eq. 2.5 is implicit, and Eqs. 2.8 and 2.9 are explicit, in the space $\mathbf{V}$.

3 The finite element space

We begin by recalling the definition of the standard Stokes finite element space that we used [3, 13]. The finite element itself is defined on a rectangle $R = (0, a) \times (0, b)$. On R, we approximate pressure as a constant and the velocity in the space $\mathbf{V}_h(R) = Q_{1,2}(R) \times Q_{2,1}(R)$, where $Q_{i,j}(R)$ are the polynomials of degree i in x_1 and degree j in x_2 defined over R. The degrees of freedom for $\mathbf{v} = (v_1, v_2) \in \mathbf{V}_h(R)$ are the 8 corner values

$$v_j(0,0)\,, \quad v_j(a,0)\,, \quad v_j(0,b)\,, \quad v_j(a,b)\,, \quad j = 1, 2\,, \tag{3.1}$$

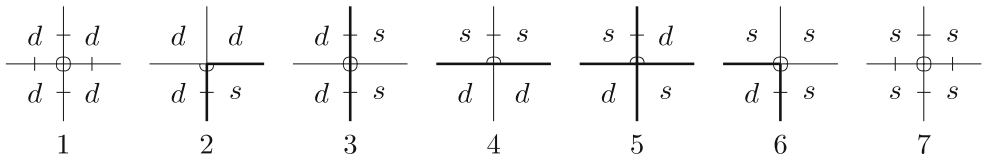

Fig. 1 The seven patterns (up to symmetries) around a corner point in the modified space $\mathbf{V}_h$. Here d represents a Darcy element, s is a Stokes element, and a heavy line is a part of Γ. For x_1 velocity components, a quarter circle in an element indicates that the corner basis function is present over the element. The corner in Pattern 5 is called a checkerboard corner. The edge tick marks indicate which edges may be used to define the corner value via the Scott–Zhang operator

and the 4 edge average normal fluxes

$$-\frac{1}{b}\int_0^b v_1(0,x_2)\,\mathrm{d}x_2\,,\quad \frac{1}{b}\int_0^b v_1(a,x_2)\,\mathrm{d}x_2\,,$$
$$-\frac{1}{a}\int_0^a v_2(x_1,0)\,\mathrm{d}x_1\,,\quad \frac{1}{a}\int_0^a v_2(x_1,b)\,\mathrm{d}x_1\,. \tag{3.2}$$

For purposes of implementation, the 4 edge degrees of freedom may be replaced by the nodal values at the midpoints of the edges; however, for easier definition of the space and for the analysis, we represent the degrees of freedom as above.

We assume henceforth that both Ω_s and Ω_d are unions of rectangles. Let $\mathcal{T}_h$ be a rectangular finite element partition of Ω, with h being the maximum element diameter, so that each element R is in either Ω_s or Ω_d. Then Γ is a union of edges of $\mathcal{T}_h$. We tacitly assume that the aspect ratio of the rectangles does not degenerate as $h \to 0$.

The standard Stokes finite element space is formed in the usual way. Let $W_h \subset W$ consist of piecewise constant functions over $\mathcal{T}_h$. Let $\tilde{\mathbf{V}}_h = \{\mathbf{v} \in \mathbf{V} \cap C(\bar{\Omega}) : \mathbf{v}|_R \in \mathbf{V}_h(R) \text{ for all } R \in \mathcal{T}_h\}$, which is formed by piecing together the elements by matching the degrees of freedom at corners and edges of the partition.

The elements of $\tilde{\mathbf{V}}_h$ must be modified near the Darcy–Stokes interface Γ since, in general, the tangential component of the velocity is not continuous there. We must remove some of the corner degrees of freedom to allow for a discontinuous tangential velocity component on Γ and simultaneously reduce the size of the polynomial space (but we must *not* degrade its approximation properties). We want to do this as simply as possible, so that there are minimal changes to a finite element code using the unmodified elements everywhere.

Around a corner point, exactly seven patterns arise, as depicted in Fig. 1. Modification is made in only three of the cases. For ease of exposition, we consider the case of horizontal, x_1-components only (x_2-components are handled similarly). If two Darcy elements share a vertical edge e and a corner on Γ, we remove the corner nodal value (which disconnects the tangential velocity). We also reduce the polynomial space by one degree on e. Thus, Pattern 2 has two modified elements on top, whereas Pattern 4 has its two lower elements modified.

Pattern 5 of Fig. 1 has alternating Stokes and Darcy elements around the corner, so we call it a *checkerboard corner*. Such corner points are problematic because the entire horizontal interface is part of Γ, which means that the x_1 velocity of the solution on the top two elements is potentially discontinuous with that on the bottom. We need to break the continuity, so we remove the corner nodal value systematically on, say, the bottom Darcy and Stokes elements.

For a corner point on $\partial\Omega$, it is trivial to examine the possibilities, as depicted in Fig. 2. If the corner point is also a corner of the domain, there is only one element containing the corner point and no modification is needed. Otherwise, the corner point is part of two elements, and modification is required only if the elements are of different types, and then only to the Darcy element, and only to the component normal to $\partial\Omega$ (i.e., tangential to Γ). Thus, only Pattern 5 in Fig. 2 is modified.

We have a grand total of 16 types of elements for each velocity component, depending on which of the four corners are affected. Removing symmetries, we are left with the seven distinct types depicted in Fig. 3. Each of these elements has degree 0, 1, or 2 on the left and right vertical edges. On $R = (0,a) \times (0,b)$, with $P_j(\xi)$ denoting polynomials in ξ of degree up to j, the polynomial spaces for x_1-components are $(a-x_1)P_i(x_2) + x_1 P_j(x_2)$, $i, j = 0, 1, 2$ [and for the x_2-

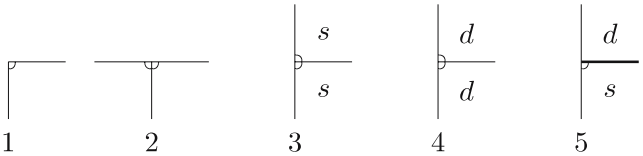

Fig. 2 The five patterns (up to symmetries) around a corner point in the modified space $\mathbf{V}_h$ on $\partial\Omega$. Here d represents a Darcy element, s is a Stokes element, unspecified is either, and a heavy line is a part of Γ. For x_1 velocity components, a quarter circle in an element indicates that the corner basis function is present over the element

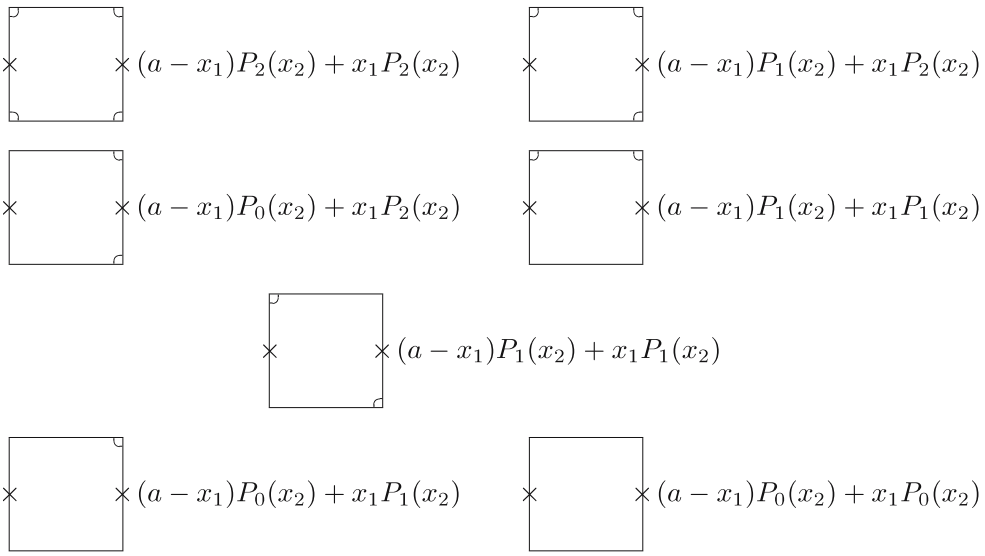

Fig. 3 The seven elements (up to symmetries) for the x_1 velocity components, on $R = (0, a) \times (0, b)$, in the modified space $\mathbf{V}_h$. The quarter circles represent corner nodal values, and the edge crosses represent normal fluxes (or, equivalently, nodal values)

components, the spaces are $P_k(x_1)(b - x_2) + P_\ell(x_1)x_2$, $k, \ell = 0, 1, 2]$. Note that in the most reduced case, the element becomes the lowest order space due to Raviart and Thomas [20].

Denote by $\mathbf{V}_h \subset \mathbf{V}$ the modified finite element space. Note that no global basis function disappears (we always have an unmodified Stokes element near Γ). Of course, the finite element method is to find $(\mathbf{u}_h, p_h) \in \mathbf{V}_h \times W_h$ such that Eqs. 2.12 and 2.13 hold for test functions $(\mathbf{v}, w)$ restricted to $\mathbf{V}_h \times W_h$. It is trivial to verify that there is a unique solution.

In a computer code, in the matrix assembly routines, one needs to check the type of element (Stokes or Darcy) to decide which of two forms is used: $2\mu(D\mathbf{u}, D\mathbf{v})_\mathrm{s}$ or $\mu(K^{-1}\mathbf{u}, \mathbf{v})_\mathrm{d}$. On a Darcy element, we need to check the nearest neighbors to decide on the local basis. When we are in contact with Γ, we also include the interface term $\mu\langle\alpha K^{-1/2}\mathbf{u}_\mathrm{s} \cdot \tau, \mathbf{v}_\mathrm{s} \cdot \tau\rangle$. Moreover, when in contact with Γ, for x_1 velocity components, we need to check the two lower corners to see if either or both are checkerboard corners (Pattern 5 of Fig. 1) and modify the local basis accordingly (we check, say, the two left-most corners for x_2 velocity components). Since the number of global basis functions is determined a priori by the number of corner points and edges, the global matrix problem has a regular sparsity pattern.

In closing this section, we note that for checkerboard corners, we could instead remove the corner nodal value altogether. However, two issues then need to be addressed. First, if a larger checkerboard pattern of Stokes and Darcy elements were to arise, so that we have an edge with checkerboard corners on both ends, then the polynomial space would drop to a constant along that edge. This would be insufficient to approximate the Stokes equations. We conclude that omitting checkerboard corner nodal values is acceptable only if such edges do not arise in the finite element partition. Second, if we indeed omit a nodal value, the sparsity structure of the matrix problem changes. Since checkerboard corner points will likely not occur in nature, it is not particularly important how we handle them. In our computer code, in fact, we ignored the issue and used the strategy that Pattern 5 of Fig. 1 is left unmodified, and only the other two Patterns 2 and 4 were treated in a special way.

4 A π operator for the velocity

We now define an important operator that will be used heavily in the next section to analyze the approximation error. For the unmodified space $\tilde{\mathbf{V}}_h$, the operator has been defined in, e.g., [3, 15]. Let $\tilde{\pi} : (H^1(\Omega))^2 \to \tilde{\mathbf{V}}_h$ denote this unmodified operator. We have the following properties [3], where $\mathcal{P}_W : L^2(\Omega) \to W_h$ denotes the L^2 projection operator and $|\cdot|_{j,\omega}$ is the usual $H^j(\omega)$ Sobolev seminorm,

$$|\psi|^2_{j,\omega} = \sum_{\alpha, |\alpha|=j} \int_\omega \left| \frac{\partial^\alpha \psi(x)}{\partial x^\alpha} \right|^2 \mathrm{d}x \,,$$

where the sum is taken over all jth-order derivatives (i.e., α runs over all multi-indices of order j). Later we will also need the usual $H^j(\omega)$ Sobolev norm $\|\cdot\|_{j,\omega}$, which is

$$\|\psi\|^2_{j,\omega} = \sum_{k=0}^{j} |\psi|^2_{k,\omega} \,.$$

We omit ω if $\omega = \Omega$, and write s or d in place of Ω_s or Ω_d.

Lemma 4.1 *Assume that* $\mathbf{v} \in (H^1(\Omega))^2$. *There exists some constant C independent of h, so that the following hold.*

(a) *The linear operator* $\tilde{\pi}$ *is bounded on* $(H^1(\Omega))^2$ *independently of h.*

(b) *For* $R \in \mathcal{T}_h$ *and* $\mathbf{v} \in (H^r(R'))^2$,

$$|\tilde{\pi}\mathbf{v} - \mathbf{v}|_{j,R} \le C|\mathbf{v}|_{r,R'} h_R^{r-j}, \quad 1 \le r \le 2, \ j = 0, 1,$$

where R' *is the union of* R *and its four nearest neighbor elements that share edges with* R, *and* $h_R = diam(R)$.

(c) *For* $\mathbf{v} \in (H^r(\Omega))^2$,

$$|\tilde{\pi}\mathbf{v} - \mathbf{v}|_j \le C|\mathbf{v}|_r h^{r-j}, \quad 1 \le r \le 2, \ j = 0, 1.$$

(d) $\mathcal{P}_W \nabla \cdot \mathbf{v} = \mathcal{P}_W \nabla \cdot \tilde{\pi}\mathbf{v}$.

By definition [3], $\tilde{\pi}$ is defined locally, element by element, as essentially the interpolant of the finite element degrees of freedom 3.1 and 3.2 (where the edge degrees of freedom must be understood as the average normal velocity component, *not* the midpoint nodal value). The only problem is that corner values are not defined for functions in $H^1(\Omega)$, so the corner nodal values are set using the Scott–Zhang operator [24]. This operator defines corner point values through integration over an adjoining edge of the finite element partition. The above results are proved by using the Trace theorem locally to relate edge integrals to area integrals. Thus, in (b), R' is larger than R and only needs to include for each corner point the element over which the area integral is computed. (We note in passing that $\tilde{\pi}$ is actually a projection because of the way the Scott–Zhang operator is defined.)

We now modify $\tilde{\pi}$ locally near Γ wherever the space $\tilde{\mathbf{V}}_h$ has been modified to form $\mathbf{V}_h$. We must begin by making a specific choice regarding the use of the Scott–Zhang operator. We apply the operator to x_1- and x_2-components of the velocity independently. Since tangential velocity components may be discontinuous across Γ, we need to define point values only using edges on which the given velocity component is continuous. Thus, we require that horizontal, x_1-component point values be defined only on vertical edges, and similarly x_2-components use only horizontal edges. Moreover, we insist that the edge chosen for the integration borders both a Darcy and a Stokes element, so the Trace theorem analysis can be taken entirely in either Ω_d or Ω_s, as needed. The only exception is when this is not possible, in which case we take the edge that borders two Stokes elements.

To illustrate the ideas, we refer to Fig. 1 and consider only x_1-components. We may choose any edge in the first and last (seventh) patterns since these do not involve Γ. We must choose a vertical edge for the other five patterns. Patterns 2 and 6 require the lower edge, and Patterns 4 and 5 require the upper edge. We can choose either vertical edge in the third pattern.

The definition of $\pi : (H^1(\Omega))^2 \to \mathbf{V}_h$ is now immediate: it is the interpolant of the modified finite element degrees of freedom of $\mathbf{V}_h$ Eqs. 3.1 and 3.2, using the Scott–Zhang operator to define corner points, using edges as noted above near Γ to avoid discontinuities in the tangential velocity.

Lemma 4.2 *Let* $R \in \mathcal{T}_h$ *and* $h_R = diam(R)$. *Suppose that* $R \subset \Omega_\ell$, *where* ℓ *is either s or d. Let* R' *be the union of* R *and its nearest neighbor elements that are also in* Ω_ℓ. *There exists some constant C independent of h, so that the following hold.*

(a) *If either* $R \subset \Omega_s$ *or* $\bar{R} \subset \Omega_d$, *and* $\mathbf{v} \in (H^r(R'))^2$, *then*

$$|\pi\mathbf{v} - \mathbf{v}|_{j,R} \le C|\mathbf{v}|_{r,R'} h_R^{r-j}, \quad 1 \le r \le 2, \ j = 0, 1.$$

(b) *If* $R \subset \Omega_d$ *and* $\partial R \cap \Gamma \neq \emptyset$, *and* $\mathbf{v} \in (H^1(R'))^2$, *then*

$$\|\pi\mathbf{v} - \mathbf{v}\|_{0,R} \le C\|\mathbf{v}\|_{1,R'} h_R.$$

(c) *For* $\mathbf{v} \in \mathbf{V}$ *such that* $\mathbf{v}_s \in (H^2(\Omega_s))^2$ *and* $\mathbf{v}_d \in (H^1(\Omega_d))^2$,

$$\|\pi\mathbf{v} - \mathbf{v}\|_{1,s} + \|\pi\mathbf{v} - \mathbf{v}\|_{0,d} \le C\{\|\mathbf{v}\|_{2,s} + \|\mathbf{v}\|_{1,d}\}h.$$

(d) $\mathcal{P}_W \nabla \cdot \mathbf{v} = \mathcal{P}_W \nabla \cdot \pi\mathbf{v}$.

Proof Result (c) follows from (a) and (b). Result (d) follows from the edge flux degrees of freedom Eq. 3.2 and a simple application of the divergence theorem:

$$\int_R \nabla \cdot \mathbf{v}\, dx = \int_{\partial R} \mathbf{v} \cdot \nu\, ds = \int_{\partial R} \pi\mathbf{v} \cdot \nu\, ds = \int_R \nabla \cdot \pi\mathbf{v}\, dx.$$

It remains only to show (a) and (b).

Suppose element $R \in \mathcal{T}_h$ is *unmodified* from that in the space $\tilde{\mathbf{V}}_h$. Since $\tilde{\pi}$ and π agree on unmodified elements, we have (a) and (b) by Lemma 4.1(b). The restriction of R' to Ω_s or Ω_d follows by treating the Scott–Zhang operator analysis from the appropriate side of each chosen edge, as discussed above and illustrated in Fig. 1.

Suppose now element $R \in \mathcal{T}_h$ is *modified* from that in the space $\tilde{\mathbf{V}}_h$. Let $\tilde{\pi}_R$ be the unmodified Stokes operator defined above, except that at corner points where a basis function was removed from R when forming $\mathbf{V}_h$, $\tilde{\pi}_R$ should be defined using an appropriate edge of R, so that it is defined over Ω_ℓ. We illustrate by referring to Fig. 1 and x_1-components. If $\ell = \mathrm{d}$ and a Pattern 2 modification arises, we use the top vertical edge to define $\tilde{\pi}_R$ for the purposes of this proof. If $\ell = \mathrm{d}$ and a Pattern 4 or 5 modification arises, or if $\ell = \mathrm{s}$ and a Pattern 5 modification arises, then we need to take the lower edge to define $\tilde{\pi}_R$ for the purposes of this proof, so $\tilde{\pi}_R$ maps onto $\tilde{\mathbf{V}}_h$.

Note that

$$\begin{aligned}\mathbf{v} - \pi\mathbf{v} &= (\mathbf{v} - \tilde{\pi}_R\mathbf{v}) + (\tilde{\pi}_R\mathbf{v} - \pi\mathbf{v}) \,, \\ &= (\mathbf{v} - \tilde{\pi}_R\mathbf{v}) + ((\tilde{\pi}_R\mathbf{v}) - \pi_R(\tilde{\pi}_R\mathbf{v})) \,,\end{aligned}$$

where π_R is the same as π except that the Scott–Zhang operator is *not* used. For Darcy elements, by Lemma 4.1, we need only show the result (b) for the operator π_R and for $\mathbf{v} = \mathbf{v}_h \in \mathbf{V}_h(R) = Q_{1,2}(R) \times Q_{2,1}(R)$. But π_R is a linear projection on the finite dimensional space $\mathbf{V}_h(R)$, so it is bounded in the $L^2(R)$ norm. Moreover, a scaling analysis shows that it is bounded independently of h. Since π_R preserves polynomials of degree 0, we have (b) by the Bramble–Hilbert lemma [7, 12]. For the modified Stokes elements, we have that π_R preserves polynomials of degree 1, so (a) follows. This completes the proof. □

5 A convergence analysis

We now present an a priori analysis of the approximation error. The analysis on Ω_d is relatively delicate and follows the ideas in [3]. Let $\hat{\mathbf{V}}_h$ be the lowest order Raviart–Thomas space, and let $\hat{\pi} : (H^1(\Omega_d))^2 \to \hat{\mathbf{V}}_h$ be the usual Raviart–Thomas projection operator [11, 20]. Among other properties, $\nabla \cdot \hat{\pi} = \mathcal{P}_W \nabla \cdot$. Let $\mathcal{P}_{\hat{\mathbf{V}}} : (L^2(\Omega_d))^2 \to \hat{\mathbf{V}}_h$ be $(L^2(\Omega_d))^2$ projection. The following lemma is shown in [3].

Lemma 5.1 *If* $\mathbf{v} \in \tilde{\mathbf{V}}_h$, *then* $\hat{\pi}\mathbf{v} = \mathcal{P}_{\hat{V}}\mathbf{v}$.

Take $\mathbf{v} \in \mathbf{V}_h$ and substitute $\hat{\pi}\mathbf{v} = \mathcal{P}_{\hat{V}}\mathbf{v}$ for $\mathbf{v}$ in Eq. 2.11 to obtain

$$\begin{aligned}&\mu(\mathcal{P}_{\hat{\mathbf{V}}}(K^{-1}\mathbf{u}), \mathbf{v})_d - (\mathcal{P}_W p, \nabla \cdot \mathbf{v})_d \\ &\quad -\langle \mathcal{P}_{\hat{\Lambda}} p_d, \mathbf{v} \cdot \nu \rangle = (\mathcal{P}_{\hat{\mathbf{V}}} f, \mathbf{v})_d \,, \end{aligned} \tag{5.1}$$

where $\mathcal{P}_{\hat{\Lambda}}$ is the projection onto piecewise constants over the interface grid of rectangle edges since $\hat{\pi}\mathbf{v} \cdot \nu$ is piecewise constant. Now combine this equation with Eqs. 2.10 and 2.13, and subtract the finite element method (2.12) and (2.13) posed over the space $\mathbf{V}_h \times W_h$ with $w \in W_h$ to obtain

$$\begin{aligned}&2\mu(D(\mathbf{u} - \mathbf{u}_h), D\mathbf{v})_s + \mu\langle \alpha K^{-1/2}(\mathbf{u}_s - \mathbf{u}_{h,s}) \cdot \tau, \mathbf{v}_s \cdot \tau \rangle \\ &\qquad + \mu(K^{-1}(\mathbf{u} - \mathbf{u}_h), \mathbf{v})_d - (\mathcal{P}_W p - p_h, \nabla \cdot \mathbf{v}) \\ &\quad = (\mathcal{P}_{\hat{\mathbf{V}}} f - f, \mathbf{v})_d + \mu(K^{-1}\mathbf{u} - \mathcal{P}_{\hat{\mathbf{V}}}(K^{-1}\mathbf{u}), \mathbf{v})_d \\ &\qquad + (p - \mathcal{P}_W p, \nabla \cdot \mathbf{v})_s - \langle p_d - \mathcal{P}_{\hat{\Lambda}} p_d, \mathbf{v} \cdot \nu \rangle \,, \end{aligned} \tag{5.2}$$

$$(\nabla \cdot (\mathbf{u} - \mathbf{u}_h), w) = 0 \,. \tag{5.3}$$

Let us take $\mathbf{v} = \pi\mathbf{u} - \mathbf{u}_h \in \mathbf{V}_h$ and $w = \mathcal{P}_W p - p_h \in W_h$. The sum of the equations leads to

$$\begin{aligned}&2\mu(D(\mathbf{u} - \mathbf{u}_h), D(\mathbf{u} - \mathbf{u}_h))_s \\ &\quad + \mu\langle \alpha K^{-1/2}(\mathbf{u}_s - \mathbf{u}_{h,s}) \cdot \tau, (\mathbf{u}_s - \mathbf{u}_{h,s}) \cdot \tau \rangle \\ &\quad + \mu(K^{-1}(\mathbf{u} - \mathbf{u}_h), (\mathbf{u} - \mathbf{u}_h))_d \\ &\quad = (\mathcal{P}_{\hat{\mathbf{V}}} f - f, \pi\mathbf{u} - \mathbf{u}_h)_d \\ &\qquad + \mu(K^{-1}\mathbf{u} - \mathcal{P}_{\hat{\mathbf{V}}}(K^{-1}\mathbf{u}), \pi\mathbf{u} - \mathbf{u}_h)_d \\ &\qquad + (p - \mathcal{P}_W p, \nabla \cdot (\pi\mathbf{u} - \mathbf{u}_h))_s \\ &\qquad - \langle p_d - \mathcal{P}_{\hat{\Lambda}} p_d, (\pi\mathbf{u} - \mathbf{u}_h) \cdot \nu \rangle \\ &\qquad + 2\mu(D(\mathbf{u} - \mathbf{u}_h), D(\mathbf{u} - \pi\mathbf{u}))_s \\ &\qquad + \mu\langle \alpha K^{-1/2}(\mathbf{u}_s - \mathbf{u}_{h,s}) \cdot \tau, (\mathbf{u}_s - \pi\mathbf{u}_s) \cdot \tau \rangle \\ &\qquad + \mu(K^{-1}(\mathbf{u} - \mathbf{u}_h), (\mathbf{u} - \pi\mathbf{u}))_d \,. \end{aligned} \tag{5.4}$$

Table 1 The numerical test cases 1–4

Case	p	$\mathbf{u}_s$	$\mathbf{u}_d$
1	0	$\begin{pmatrix} 0 \\ \frac{1}{2} - y^2 \end{pmatrix}$	$\begin{pmatrix} 0 \\ 0 \end{pmatrix}$
2	$e^x \sin(x+y)$	$\begin{pmatrix} \cos(xy) \\ e^{x+y} \end{pmatrix}$	$\begin{pmatrix} \cos(xy) \\ 0 \end{pmatrix}$
3	$\cos(x^2 y)$	$\begin{pmatrix} \sin(x^2 y) \\ \cos(x^2 y) \end{pmatrix}$	$\begin{pmatrix} \sin(x^2 y) \\ e^{x+y} \end{pmatrix}$
4	$-y^4 e^x$	$\begin{pmatrix} y^4 e^x \\ e^y \cos(2x) \end{pmatrix}$	$\begin{pmatrix} y^4 e^x \\ 4y^3 e^x \end{pmatrix}$

Table 2 Observed convergence rates using the unmodified space $\tilde{\mathbf{V}}_h$ for the errors $E_p = p - p_h$ and $E_{\mathbf{u}} = \mathbf{u} - \mathbf{u}_h$ for test cases 1–4 on a uniform grid

Case	$\|E_p\|_0$	$\|\mathcal{P}_W E_p\|_0$	$\|E_{\mathbf{u}}\|_0$	$\|\nabla E_{\mathbf{u}}\|_0$	$\|\nabla \cdot E_{\mathbf{u}}\|_0$
1	1.2081	1.2081	0.5084	–0.4986	0.5298
2	0.9997	0.9690	0.4982	–0.5032	0.5196
3	1.0082	1.0780	0.5003	–0.5054	0.5174
4	0.9961	1.0161	0.5618	–0.4743	0.6228

Since $|\nabla \cdot \mathbf{v}| \le |D\mathbf{v}|$, for some $\epsilon > 0$ as small as we like and $C > 0$, it is straightforward to estimate

$$\begin{aligned}
&\|D(\mathbf{u} - \mathbf{u}_h)\|_{0,\mathrm{s}}^2 + \|(\mathbf{u}_\mathrm{s} - \mathbf{u}_{h,\mathrm{s}}) \cdot \tau\|_{0,\Gamma}^2 + \|\mathbf{u} - \mathbf{u}_h\|_{0,\mathrm{d}}^2 \\
&\quad \le C\Big\{\|\mathcal{P}_{\hat{\mathbf{V}}} f - f\|_{0,\mathrm{d}}^2 + \|K^{-1}\mathbf{u} - \mathcal{P}_{\hat{\mathbf{V}}}(K^{-1}\mathbf{u})\|_{0,\mathrm{d}}^2 \\
&\qquad + \|p - \mathcal{P}_W p\|_{0,\mathrm{s}}^2 + \|p_\mathrm{d} - \mathcal{P}_{\hat{\Lambda}} p_\mathrm{d}\|_{0,\Gamma}^2 \\
&\qquad + \|D(\mathbf{u} - \pi\mathbf{u})\|_{0,\mathrm{s}}^2 + \|\mathbf{u} - \pi\mathbf{u}\|_{0,\mathrm{d}}^2 \\
&\qquad + \|(\mathbf{u}_\mathrm{s} - \pi\mathbf{u}_\mathrm{s}) \cdot \tau\|_{0,\Gamma}^2\Big\} \\
&\qquad + \epsilon\|\pi\mathbf{u} - \mathbf{u}_h\|_{1,\mathrm{s}}^2 \,. \qquad (5.5)
\end{aligned}$$

We require a Korn inequality for $\mathbf{V}$.

Lemma 5.2 *If ω is a Lipschitz domain and $\mathbf{v} \in (H^1(\omega))^2$, then there is some constant C such that*

$$\|\mathbf{v}\|_{1,\omega} \le C\Big\{\|D\mathbf{v}\|_{0,\omega} + \|\mathbf{v} \cdot \tau\|_{0,\partial\omega}\Big\} \,.$$

Proof We use a relatively standard proof by contradiction technique for proving this variant of Korn's inequality (see, e.g., [10, Proof of Theorem 9.2.16]). The proof is based on the direct sum decomposition

$$(H^1(\omega))^2 = H \oplus R \,,$$

where

$$\begin{aligned}
H = \Bigg\{\mathbf{v} \; &= (v_1, v_2) \in (H^1(\omega))^2 : \int_\omega \mathbf{v}\,\mathrm{d}x \\
&= \int_\omega \left(\frac{\partial v_1}{\partial x_2} - \frac{\partial v_2}{\partial x_1}\right)\mathrm{d}x = 0\Bigg\}
\end{aligned}$$

are the rotation free vectors and

$$R = \mathrm{span}\left\{\begin{pmatrix}1\\0\end{pmatrix}, \begin{pmatrix}0\\1\end{pmatrix}, \begin{pmatrix}-x_2\\x_1\end{pmatrix}\right\}$$

are the infinitesimal rigid motions.

Following the standard proof (as in [10, Proofs of Theorem. 9.2.16 and Corollary 9.2.22]), we are led to the following requirement: If $\mathbf{v} \in R$ and $\mathbf{v} \cdot \tau = 0$, then $\mathbf{v} = 0$. Since $\mathbf{v} = (c_1 - b x_2, c_2 + b x_1)$, Stokes theorem immediately implies that $b = 0$. But then $\mathbf{v}$ is constant, and the result is trivial. □

Thus, we can bound the left side of Eq. 5.5 from below by a multiple of $\|\mathbf{u} - \mathbf{u}_h\|_{1,\mathrm{s}}^2 + \|\mathbf{u} - \mathbf{u}_h\|_{0,\mathrm{d}}^2$. Applying standard approximation results for the various projection operators, we are led to the error estimate

$$\begin{aligned}
&\|\mathbf{u} - \mathbf{u}_h\|_{1,\mathrm{s}} + \|\mathbf{u} - \mathbf{u}_h\|_{0,\mathrm{d}} \\
&\quad \le Ch\Big\{\|f\|_{1,\mathrm{d}} + \|\mathbf{u}\|_{2,\mathrm{s}} + \|\mathbf{u}\|_{1,\mathrm{d}} + \|p\|_{1,\mathrm{s}} + \|p_\mathrm{d}\|_{1,\Gamma}\Big\} \,. \qquad (5.6)
\end{aligned}$$

We also prove an estimate for the pressure. Let $\mathbf{v} \in (H^1(\Omega))^2$ satisfy $\nabla \cdot \mathbf{v} = p - p_h$ and $\|\mathbf{v}\|_1 \le C\|p - p_h\|_0$; such a $\mathbf{v}$ exists by [4]. Substitute $\pi\mathbf{v} \in \mathbf{V}_h$ as test function in Eq. 5.2, and note that $\mathcal{P}_W \nabla \cdot \pi\mathbf{v} = \mathcal{P}_W p - p_h$. We are led to the estimate

$$\begin{aligned}
\|p - p_h\|_0^2 \le C\Big\{&\|\mathbf{u} - \mathbf{u}_h\|_{1,\mathrm{s}} + \|\mathbf{u} - \mathbf{u}_h\|_{0,\mathrm{d}} \\
&+ \|\mathcal{P}_{\hat{\mathbf{V}}} f - f\|_{0,\mathrm{d}}^2 + \|K^{-1}\mathbf{u} \\
&- \mathcal{P}_{\hat{\mathbf{V}}}(K^{-1}\mathbf{u})\|_{0,\mathrm{d}}^2 \\
&+ \|p - \mathcal{P}_W p\|_0^2 + \|p_\mathrm{d} - \mathcal{P}_{\hat{\Lambda}} p_\mathrm{d}\|_{0,\Gamma}^2\Big\} \\
&+ \epsilon\Big\{\|\pi\mathbf{v}\|_{1,\mathrm{s}}^2 + \|\pi\mathbf{v}\|_{0,\mathrm{d}}^2\Big\} \,, \qquad (5.7)
\end{aligned}$$

where again $\epsilon > 0$ is as small as we wish. Now π is bounded on $(H^1(\Omega_\mathrm{s}))^2$, so

$$\|\pi\mathbf{v}\|_{1,\mathrm{s}} \le C\|\mathbf{v}\|_{1,\mathrm{s}} \le C\|p - p_h\|_0 \,,$$

and

$$\begin{aligned}
\|\pi\mathbf{v}\|_{0,\mathrm{d}} &\le \|\mathbf{v}\|_{0,\mathrm{d}} + \|\mathbf{v} - \pi\mathbf{v}\|_{0,\mathrm{d}} \\
&\le \|\mathbf{v}\|_{0,\mathrm{d}} + Ch\|\mathbf{v}\|_{1,\mathrm{d}} \le C\|p - p_h\|_0 \,,
\end{aligned}$$

so we can remove the last two terms on the right side of Eq. 5.7 and apply standard approximation results.

Table 3 Observed convergence rates using the modified space $\mathbf{V}_h$ for the errors $E_p = p - p_h$ and $E_{\mathbf{u}} = \mathbf{u} - \mathbf{u}_h$ for test cases 1–4 on a uniform grid

Case	$\|E_p\|_0$	$\|\mathcal{P}_W E_p\|_0$	$\|E_{\mathbf{u}}\|_0$	$\|\nabla E_{\mathbf{u}}\|_0$	$\|\nabla E_{\mathbf{u}}\|_{0,s}$	$\|\nabla \cdot E_{\mathbf{u}}\|_0$
1	2.004	2.004	2.001	1.000	1.000	1.000
2	1.001	1.509	1.431	0.431	1.258	0.975
3	1.060	1.610	1.431	0.419	1.002	0.982
4	1.038	1.703	1.437	0.412	1.037	0.965

Table 4 Observed convergence rates using the modified space $\mathbf{V}_h$ for the errors $E_p = p - p_h$ and $E_{\mathbf{u}} = \mathbf{u} - \mathbf{u}_h$ for test cases 1–4 on a randomly perturbed grid

Case	$\|E_p\|_0$	$\|\mathcal{P}_W E_p\|_0$	$\|E_{\mathbf{u}}\|_0$	$\|\nabla E_{\mathbf{u}}\|_0$	$\|\nabla E_{\mathbf{u}}\|_{0,s}$	$\|\nabla \cdot E_{\mathbf{u}}\|_0$
1	1.983	1.983	1.963	0.988	0.988	0.988
2	0.987	1.458	1.137	0.114	1.239	0.616
3	1.038	1.596	1.157	0.114	0.999	0.682
4	1.006	1.664	1.173	0.159	1.024	0.781

Collecting this estimate, Eq. 5.6, and using Eq. 5.3, we have the following theorem.

Theorem 5.3 *There is some constant C such that*

$$\begin{aligned}\|\mathbf{u} - \mathbf{u}_h\|_{1,s} + \|\mathbf{u} - \mathbf{u}_h\|_{0,d} + \|p - p_h\|_0 \\ \le Ch\big\{\|f\|_{1,d} + \|\mathbf{u}\|_{2,s} + \|\mathbf{u}\|_{1,d} \\ + \|p\|_{1,s} + \|p\|_{1,d} + \|p_d\|_{1,\Gamma}\big\}\,.\end{aligned}$$

Moreover, $\mathcal{P}_W \nabla \cdot \mathbf{u}_h = \mathcal{P}_W q$.

6 Some numerical results

We present some simple test cases involving smooth solutions to verify the convergence rates. Additional numerical examples related to simulation of flow in vuggy porous media can be found in [1]. For simplicity, in all our examples, Ω is the unit square and $\alpha = \mu = K = 1$.

6.1 A remark on the solution procedure

As noted earlier in Section 3, the resulting linear system is symmetric and has a completely regular structure. However, the matrix is quite ill-conditioned; moreover, it has a saddle-point structure. We briefly remark on our solution strategy, which is very effective for problems up to grid sizes of perhaps 128×128. We chose to implement a solver for the scheme using an inexact Uzawa technique [8, 9]. For a rectangular grid with $n_x \times n_y$ elements, the matrix problem is of the form

$$\begin{bmatrix} A_{xx} & A_{xy} & B_x \\ A_{xy}^{\mathrm{T}} & A_{yy} & B_y \\ B_x^{\mathrm{T}} & B_y^{\mathrm{T}} & 0 \end{bmatrix} \begin{bmatrix} u_x \\ u_y \\ p \end{bmatrix} = \begin{bmatrix} f_x \\ f_y \\ q \end{bmatrix},$$

where u_x represents the $(n_x + 1)(2n_y + 1)$ nodal values of the x_1 velocity components $\mathbf{v}_i^x$, u_y represents the $(2n_x + 1)(n_y + 1)$ nodal values of the x_2 velocity components $\mathbf{v}_i^y$, and p represents the $n_x n_y$ nodal values of the pressure.

Except for modification for boundary conditions,

$$\begin{aligned} A_{xx,ij} &= 2\mu(D\mathbf{v}_i^x, D\mathbf{v}_j^x)_{\mathrm{s}} + \mu\langle\alpha K^{-1/2}\mathbf{v}_{\mathrm{s},i}^x \cdot \tau, \mathbf{v}_{\mathrm{s},j}^x \cdot \tau\rangle \\ &\quad + \mu(K^{-1}\mathbf{v}_i^x, \mathbf{v}_j^x)_{\mathrm{d}}\,, \\ A_{yy,ij} &= 2\mu(D\mathbf{v}_i^y, D\mathbf{v}_j^y)_{\mathrm{s}} + \mu\langle\alpha K^{-1/2}\mathbf{v}_{\mathrm{s},i}^y \cdot \tau, \mathbf{v}_{\mathrm{s},j}^y \cdot \tau\rangle \\ &\quad + \mu(K^{-1}\mathbf{v}_i^y, \mathbf{v}_j^y)_{\mathrm{d}}\,, \\ A_{xy,ij} &= 2\mu(D\mathbf{v}_i^x, D\mathbf{v}_j^y)_{\mathrm{s}}\,, \end{aligned}$$

so both A_{xx} and A_{yy} are positive definite. Since these submatrices arise from a two-dimensional rectangular grid, they are banded with a reasonable band size, so direct factorization is feasible for problems not too large.

The inexact Uzawa procedure starts with an initial guess for the solution, say $p^0 = 0$, $\mathbf{u}_x^0 = 0$, and $\mathbf{u}_y^0 = 0$, and then for $\ell = 1, 2, \ldots$, it defines iteratively

$$\mathbf{u}_x^\ell = A_{xx}^{-1}(f_x - A_{xy}\mathbf{u}_y^{\ell-1} - B_x p^{\ell-1})\,, \tag{6.1}$$

$$\mathbf{u}_y^\ell = A_{yy}^{-1}(f_y - A_{xy}^{\mathrm{T}}\mathbf{u}_x^{\ell-1} - B_y p^{\ell-1})\,, \tag{6.2}$$

$$p^\ell = p^{\ell-1} + \beta M(B_x^{\mathrm{T}}\mathbf{u}_x + B_y^{\mathrm{T}}\mathbf{u}_y - q)\,, \tag{6.3}$$

where $\beta > 0$ is the Uzawa parameter and M is some preconditioner for the system.

Table 5 The numerical test cases 5 and 6

Case	p_{s}	p_{d}	$\mathbf{u}_{\mathrm{s}}$	$\mathbf{u}_{\mathrm{d}}$	$(\frac{1}{2}, 1) \times (0, \frac{1}{2})$
5	$\mathrm{e}^{-2xy} - \frac{1}{2}\mathrm{e}^{-1/2}$	0	$\begin{pmatrix} x\mathrm{e}^{-y} + \frac{1}{2}\mathrm{e}^{-x} \\ y\mathrm{e}^{-x} + \frac{1}{2}\mathrm{e}^{-y} \end{pmatrix}$	$\begin{pmatrix} x(\mathrm{e}^{-2xy} + \mathrm{e}^{-x}) \\ y(4y^2\mathrm{e}^{-x} + \mathrm{e}^{-y}) \end{pmatrix}$	Ω_{d}
6	$2\mathrm{e}^{-y}$	0	$\begin{pmatrix} (2x+1)\mathrm{e}^{-y} \\ -2\mathrm{e}^{-y} \end{pmatrix}$	$\begin{pmatrix} 2\mathrm{e}^{-2xy} \\ (y - \frac{1}{2})^3\mathrm{e}^{-x} - 2\mathrm{e}^{-1/2} \end{pmatrix}$	Ω_{s}

Table 6 Observed convergence rates using the modified space $\mathbf{V}_h$ for the errors $E_p = p - p_h$ and $E_{\mathbf{u}} = \mathbf{u} - \mathbf{u}_h$ for test cases 5 and 6

Case	$\|E_p\|_0$	$\|\mathcal{P}_W E_p\|_0$	$\|E_{\mathbf{u}}\|_0$	$\|\nabla E_{\mathbf{u}}\|_0$	$\|\nabla E_{\mathbf{u}}\|_{0,s}$	$\|\nabla \cdot E_{\mathbf{u}}\|_0$	Grid
5	1.000	2.066	2.005	1.007	1.033	1.004	Uniform
6	1.001	1.895	1.993	1.007	1.005	1.000	Uniform
5	1.000	1.988	2.006	1.011	1.004	1.011	Perturbed
6	1.000	1.771	1.983	1.003	0.999	1.000	Perturbed

A relatively good preconditioner is needed. We took

$$M = \left[\begin{pmatrix} B_x^{\mathrm{T}} & B_y^{\mathrm{T}} \end{pmatrix} \begin{pmatrix} A_{xx}^{-1} & 0 \\ 0 & A_{yy}^{-1} \end{pmatrix} \begin{pmatrix} B_x \\ B_y \end{pmatrix} \right]^{-1}, \tag{6.4}$$

which is invertible (after modification for the compatibility condition that p is defined only up to a constant). This computation is quite expensive since the matrix is full, but again, direct factorization is feasible for problems not too large. (For larger problems, some inexact inverse could be used.) This preconditioner is exact when $A_{xy} = 0$ and $\beta = 1$. We found that the Jacobi preconditioner given by inverting only the diagonal of Eq. 6.4 performed very poorly, requiring sometimes hundreds of thousands of iterations to converge and worsening greatly with the size of the problem. On the other hand, M solved problems on grids of size 8×8 up to 64×64 using only around 100 iterations (the worse case took under 500 iterations).

This preconditioner is very expensive for larger problems, and more research is needed to improve the linear system solution methodology.

6.2 Some simply constructed examples

In our first set of examples, $\Omega_{\mathrm{s}} = (0, 1/2) \times (0, 1)$, $\Omega_{\mathrm{d}} = (1/2, 1) \times (0, 1)$, and Γ is the line $x = 1/2$. It is difficult to construct solutions that satisfy the entire Darcy–Stokes system (2.1)–(2.9). If $\mathbf{u}$ and p are chosen somehow, we can easily satisfy Eqs. 2.1–2.4 by defining f and q appropriately. Moreover, rather than requiring the solution to satisfy the outer boundary conditions (2.8) and (2.9), we can simply allow for a more general and nonhomogeneous set; again, the nonhomogeneous terms are defined from the solution.

Table 7 The numerical test cases 7 and 8

Case	p_{s}	p_{d}	$\mathbf{u}_{\mathrm{s}}$	$\mathbf{u}_{\mathrm{d}}$
7	0	0	$\begin{pmatrix} \frac{1}{4}(-2y^2 + y + 1) \\ 0 \end{pmatrix}$	$\begin{pmatrix} 1 \\ 0 \end{pmatrix}$
8	y	$1 - y$	$\begin{pmatrix} 0 \\ 2 \end{pmatrix}$	$\begin{pmatrix} 0 \\ 2 \end{pmatrix}$

The difficulty is finding a solution satisfying the interface conditions (2.5)–(2.7). In this subsection, we simply use the same trick of generalizing the equations to include a nonhomogeneous term. That is, we replace Eqs. 2.6 and 2.7 by

$$2\nu \cdot D\mathbf{u}_{\mathrm{s}} \cdot \tau = -\alpha K^{-1/2} \mathbf{u}_{\mathrm{s}} \cdot \tau + g_1 \quad \text{on } \Gamma, \tag{6.5}$$

$$2\mu\nu \cdot D\mathbf{u}_{\mathrm{s}} \cdot \nu = p_{\mathrm{s}} - p_{\mathrm{d}} + g_2 \quad \text{on } \Gamma. \tag{6.6}$$

The construction is now clear: choose $\mathbf{u}$ satisfying Eq. 2.5, and then define f, q, g_1, g_2, and the outer boundary conditions from the solution. These test cases are summarized in Table 1. The variational form for this modified system has only a small change: Eq. 2.12 now includes the two terms $\langle g_2, \mathbf{v} \cdot \nu \rangle + \mu \langle g_1, \mathbf{v}_{\mathrm{s}} \cdot \tau \rangle$ on the right side.

If we use the unmodified finite element space $\tilde{\mathbf{V}}_h$ of Fortin [3, 13], we see poor convergence results in Table 2. This is due to the fully continuous approximation of the velocity. However, our constructed solutions have a discontinuity in $\mathbf{u} \cdot \tau$ on Γ. The modified space $\mathbf{V}_h$ defined in Section 3 corrects this defect, as seen by the convergence rates in Tables 3 and 4.

In Table 3, we have used uniform grids of size 8×8, 16×16, 32×32, and 64×64. In Table 4, we have randomly perturbed the points of the uniform grid by plus or minus one quarter of the uniform cell spacing, except that the center lines have been unperturbed so as to resolve Γ. We clearly see at least $O(h)$ convergence for the pressure and velocity as measured in the L^2-norm, and at least $O(h)$ convergence for the gradient of the velocity on Ω_{s}, as proved in Theorem 5.3. In fact, we see more from these computational results. It appears that there is some superconvergence of order perhaps $O(h^{3/2})$ for the error $\mathcal{P}_W p - p_h$ in the L^2-norm, although it is not the usual $O(h^2)$ that mixed methods often produce. Moreover, on uniform grids only, we see perhaps $O(h^{1/2})$ convergence in the L^2-norm of $\nabla(\mathbf{u} - \mathbf{u}_h)$ over all of Ω. Such convergence was observed for the unmodified elements when solving Darcy systems on uniform grids (see [3]). Finally, we see convergence in the L^2-norm of $\nabla \cdot (\mathbf{u} - \mathbf{u}_h)$ of order perhaps $O(h)$ on uniform grids and $O(h^{1/2})$ in general.

Table 8 Observed convergence rates using the modified space $\mathbf{V}_h$ for the errors $E_p = p - p_h$ and $E_\mathbf{u} = \mathbf{u} - \mathbf{u}_h$ for test case 8

Case	$\|E_p\|_0$	$\|\mathcal{P}_W E_p\|_0$	$\|E_\mathbf{u}\|_0$	$\|\nabla E_\mathbf{u}\|_0$	$\|\nabla E_\mathbf{u}\|_{0,s}$	$\|\nabla \cdot E_\mathbf{u}\|_0$	Grid
8	1.000	—	2.415	1.424	1.424	2.000	Uniform
8	0.988	—	2.482	1.449	1.449	1.977	Perturbed

6.3 Some smooth examples with corners

In our second set of examples, we take $\Gamma = \big(\{1/2\} \times (0, 1/2]\big) \cup \big([1/2, 1) \times \{1/2\}\big)$. That is, Γ has a corner and separates off the lower right quarter of the square $(1/2, 1) \times (0, 1/2)$, which will be Ω_d in test case 5 and Ω_s in test case 6. Note that test case 6 uses a modified element near the central corner (see Fig. 1, Pattern 2). Overall, these two cases require all modification patterns depicted in Fig. 1, except for the checkerboard Pattern 5.

In this set of examples, we fully satisfy the system (2.1)–(2.7). We handle Eqs. 2.1–2.4 by defining f and q and the external boundary conditions (2.8) and (2.9) as above, once $\mathbf{u}$ and p are fixed. We first choose some $\mathbf{u}_\mathrm{s}$ satisfying Eq. 2.6 and then take p_d constant and find some p_s that satisfies Eq. 2.7. Finally, $\mathbf{u}_\mathrm{d}$ is chosen to satisfy Eq. 2.5. Our test cases are summarized in Table 5.

From Table 6, we see very good convergence. Actually, the L^2 and H^1 errors for $\mathbf{u} - \mathbf{u}_h$ are somewhat better than expected. We see clearly from these two test cases that there is no convergence difficulty with modifying the basis over a Darcy element.

6.4 Some simple layered examples

In our last set of examples, $\Omega_\mathrm{s} = (0, 1) \times (0, 1/2)$, $\Omega_\mathrm{d} = (0, 1) \times (1/2, 1)$, and Γ is the line $y = 1/2$. We use the analytical solution of [2]. These test cases are summarized in Table 7.

Test case 7 has a solution $(p, \mathbf{u})$ that is in the finite dimensional space $\mathbf{V}_h$, so it is solved exactly up to rounding error. The solution to test case 8 is not in the space, and only $p_h = \mathcal{P}_W p$ is computed exactly. However, as shown in Table 8, the convergence is as good as or better than that expected from the earlier test cases.

7 A lower dimension modification

In this section, we further modify $\mathbf{V}_h$ so that extra tangential continuity is removed from the Darcy side of the space. That is, remove the corner degrees of freedom 3.1 whenever the corner has Darcy elements surrounding it (see Fig. 1 – we modify only Pattern 1). Call the resulting space $\bar{\mathbf{V}}_h$. The effect is to use Raviart–Thomas elements $\hat{\mathbf{V}}_h$ strictly inside Ω_d, the full Fortin Stokes elements $\tilde{\mathbf{V}}_h$ strictly inside Ω_s, and our modified elements $\mathbf{V}_h$ as transition elements near Γ. We may lose some global basis functions and therefore also the regular sparsity structure of the matrix (although this regular structure can be recovered with some so-called "slave nodes" that are set to zero if desired).

The definition of the operator $\bar{\pi} : (H^1(\Omega))^2 \to \bar{\mathbf{V}}_h$ is defined analogously as to that in Section 4, and a similar error estimate to Lemma 4.2 holds. Moreover, an a priori error analysis will yield a result analogous to Theorem 5.3.

In Tables 9 and 10, we show the convergence of this modified scheme. These test cases are the same as in the previous section, but note that we omit the

Table 9 Observed convergence rates using the modified space $\bar{\mathbf{V}}_h$ for the errors $E_p = p - p_h$ and $E_\mathbf{u} = \mathbf{u} - \mathbf{u}_h$ for test cases 1–6 and 8 on a uniform grid

Case	$\|E_p\|_0$	$\|\mathcal{P}_W E_p\|_0$	$\|E_\mathbf{u}\|_0$	$\|\nabla E_\mathbf{u}\|_{0,s}$	$\|\nabla \cdot E_\mathbf{u}\|_0$
1	2.004	2.004	2.001	1.000	1.000
2	1.000	1.936	0.994	1.262	0.801
3	1.009	1.950	1.000	1.002	0.971
4	1.011	1.925	0.998	1.054	0.914
5	1.006	1.787	0.993	1.037	0.739
6	1.001	1.920	0.969	1.005	0.560
8	1.000	—	2.415	1.424	2.000

Table 10 Observed convergence rates using the modified space $\bar{\mathbf{V}}_h$ for the errors $E_p = p - p_h$ and $E_\mathbf{u} = \mathbf{u} - \mathbf{u}_h$ for test cases 1–6 and 8 on a randomly perturbed grid

Case	$\|E_p\|_0$	$\|\mathcal{P}_W E_p\|_0$	$\|E_\mathbf{u}\|_0$	$\|\nabla E_\mathbf{u}\|_{0,s}$	$\|\nabla \cdot E_\mathbf{u}\|_0$
1	1.983	1.983	1.963	0.988	0.988
2	0.986	2.041	0.971	1.243	0.802
3	0.996	2.141	0.986	0.998	0.962
4	0.982	1.935	0.975	1.042	0.903
5	1.006	1.712	0.990	1.008	0.740
6	1.001	1.812	0.955	1.000	0.567
8	0.988	—	2.482	1.449	1.977

H^1 errors on Ω since now there are discontinuities in Ω_d and no convergence can be expected. We also do not show convergence rates for test case 7 because it is essentially solved exactly up to rounding error. We see the expected convergence rates of at least $O(h)$ for the pressure and velocity as measured in the L^2-norm, and at least $O(h)$ convergence for the gradient of the velocity on Ω_s, as proved in the analogue to Theorem 5.3. It appears that there is some superconvergence of order perhaps $O(h^2)$ for the error $\mathcal{P}_W p - p_h$ in the L^2-norm. Finally, we see convergence in the L^2-norm of $\nabla \cdot (\mathbf{u} - \mathbf{u}_h)$ of order perhaps only order $O(h^{1/2})$ in general. There does not appear to be any advantage to using a uniform grid.

These rates are consistent with those from the previous scheme using $\mathbf{V}_h$, except that previously the $\mathcal{P}_W p - p_h$ error only converged at the rate $O(h^{3/2})$. The magnitude of the pressure errors in the L^2-norm was very comparable. However, the velocity and divergence errors are a bit better for the previous scheme. This would be expected since the velocity polynomial space of $\mathbf{V}_h$ is somewhat richer on Ω_d than that of $\bar{\mathbf{V}}_h$. The solution time of the two schemes is also very comparable. Thus, although the modification of the finite element space $\bar{\mathbf{V}}_h$ in this section results in a smaller space and is simple to implement, it does not appear to be better than the previous space $\mathbf{V}_h$.

Acknowledgements This work was supported by the US National Science Foundation under grant DMS-0074310 and DMS-0417431.

References

1. Arbogast, T., Brunson, D.S., Bryant, S.L., Jennings, J.W.: A preliminary computational investigation of a macro-model for vuggy porous media. In: Miller, C.T. et al. (eds.) Computational Methods in Water Resources XV. Elsevier , New York (2004)
2. Arbogast, T., Lehr, H.L.: Homogenization of a Darcy-Stokes system modeling vuggy porous media. Comput. Geosci. **10**, 291–302 (2006)
3. Arbogast, T., Wheeler, M.F.: A family of rectangular mixed elements with a continuous flux for second order elliptic problems. SIAM J. Numer. Anal. **42**, 1914–1931 (2005)
4. Arnold, D.N., Scott, L.R., Vogelius, M.: Regular inversion of the divergence operator with Dirichlet boundary conditions on a polygon. Ann. Sc. Norm. Super. Pisa Cl. Sci.-Ser. IV **XV**, 169–192 (1988)
5. Beavers, G.S., Joseph, D.D.: Boundary conditions at a naturally permeable wall. J. Fluid Mech. **30**, 197–207 (1967)
6. Bensoussan, A., Lions, J.L., Papanicolaou, G.: Asymptotic Analysis for Periodic Structure. North-Holland, Amsterdam (1978)
7. Bramble, J.H., Hilbert, S.R.: Estimation of linear functionals on Sobolev spaces with applications to Fourier transforms and spline interpolation. SIAM J. Numer. Anal. **7**, 112–124 (1970)
8. Bramble, J.H., Pasciak, J.E.: A preconditioning technique for indefinite systems resulting from mixed approximations of elliptic problems. Math. Comput. **50**, 1–17 (1988)
9. Bramble, J.H., Pasciak, J.E., Vassilev, A.T.: Analysis of the inexact Uzawa algorithm for saddle point problems. SIAM J. Numer. Anal. **34**, 1072–1092 (1997)
10. Brenner, S.C., Scott, L.R.: The Mathematical Theory of Finite Element Methods. Springer-Verlag, Berlin Heidelberg New York (1994)
11. Brezzi, F., Fortin, M.: Mixed and Hybrid Finite Element Methods. Springer, Berlin Heidelberg New York (1991)
12. Dupont, T., Scott, L.R.: Polynomial approximation of functions in Sobolev space. Math. Comput. **34**, 441–463 (1980)
13. Fortin, M.: Old and new finite elements for incompressible flows. Int. J. Numer. Methods Fluids **1**, 347–364 (1981)
14. Gartling, D.K., Hickox, C.E., Givler, R.C.: Simulation of coupled viscous and porous flow problems. Comput. Fluid Dyn. **7**, 23–48 (1996)
15. Girault, V., Raviart, P.A.: Finite Element Methods for Navier–Stokes Equations: Theory and Algorithms. Springer-Verlag, Berlin Heidelberg New York (1986)
16. Hornung, U. (ed.): Homogenization and Porous Media, Interdisciplinary Applied Mathematics Series. Springer-Verlag, Berlin Heidelberg New York (1997)
17. Jikov, V.V., Kozlov, S.M., Oleinik, O.A.: Homogenization of Differential Operators and Integral Functions. Springer-Verlag, Berlin Heidelberg New York (1994)
18. Jones, I.P.: Low Reynolds number flow past a porous spherical shell. Proc. Camb. Philos. Soc. **73**, 231–238 (1973)
19. Layton, W.J., Schieweck, F., Yotov, I.: Coupling fluid flow with porous media flow. SIAM J. Numer. Anal. **40**, 2195–2218 (2003)
20. Raviart, R.A., Thomas, J.M.: A mixed finite element method for 2nd order elliptic problems. In: Galligani, I., Magenes, E. (eds.) Mathematical Aspects of Finite Element Methods, No. 606 in Lecture Notes in Math, pp. 292–315. Springer-Verlag, Berlin Heidelberg New York (1977)
21. Saffman, P.G.: On the boundary condition at the interface of a porous medium. Stud. Appl. Math. **1**, 93–101 (1971)
22. Salinger, A.G., Aris, R., Derby, J.J.: Finite element formulations for large-scale, coupled flows in adjacent porous and open fluid domains. Int. J. Numer. Methods Fluids **18**, 1185–1209 (1994)
23. Sanchez-Palencia, E.: Non-homogeneous Media and Vibration Theory. no. 127 in Lecture Notes in Physics. Springer-Verlag, Berlin Heidelberg New York (1980)
24. Scott, L.R., Zhang, S.: Finite element interpolation of nonsmooth functions satisfying boundary conditions. Math. Comput. **54**, 483–493 (1990)